Large piezoelectricity and dielectric permittivity in $BaTiO_3$-$xBaSnO_3$ system: The role of phase coexisting

2012 EPL 98 27008

(http://iopscience.iop.org/0295-5075/98/2/27008)

A Letters Journal Exploring the Frontiers of Physics

April 2012

EPL, **98** (2012) 27008
doi: 10.1209/0295-5075/98/27008

www.epljournal.org

Large piezoelectricity and dielectric permittivity in $BaTiO_3$-$xBaSnO_3$ system: The role of phase coexisting

Yonggang Yao[1], Chao Zhou[1], Duchao Lv[1], Dong Wang[1], Haijun Wu[1], Yaodong Yang[1(a)] and Xiaobing Ren[1,2(b)]

[1] *Multi-disciplinary Materials Research Center, Frontier Institute of Science and Technology, Xian Jiaotong University - Xi'an 710049, China*
[2] *Ferroic Physics Group, National Institute for Materials Science - Tsukuba 305-0047, Ibaraki, Japan*

received 17 February 2012; accepted in final form 26 March 2012
published online 30 April 2012

PACS 77.22.-d – Dielectric properties of solids and liquids
PACS 77.65.Bn – Piezoelectric and electrostrictive constants

Abstract – We report ultrahigh dielectric and piezoelectric properties in $BaTiO_3$-$xBaSnO_3$ ceramics at its quasi-quadruple point, a point where four phases (Cubic-Tetragonal-Orthorhombic-Rhombohedral) nearly coexist together in the temperature-composition phase diagram. At this point, dielectric permittivity reaches ~ 75000, a 6–7-fold increase compared with that of pure $BaTiO_3$ at its Curie point; the piezoelectric coefficient d_{33} reaches 697 pC/N, 5 times higher than that of pure $BaTiO_3$. Also, a quasi-quadruple point system exhibits double morphotropic phase boundaries, which can be used to reduce the temperature and composition sensitivity of its high piezoelectric properties. A Landau-Devonshire model shows that four-phase coexisting leading to minimizing energy barriers for both polarization rotation and extension might be the origin of giant dielectric and piezoelectric properties around this point.

Ferroelectric materials with large permittivity and piezoelectricity are widely utilized in various devices, such as capacitors, piezoelectric sensors and actuators [1–3]. The common way to promote the permittivity and piezoelectricity (hereafter denoted as AC properties) is to place materials at their phase transition boundaries. For example, a paraelectric to ferroelectric (or a relaxor) phase boundary can greatly enhance the permittivity [4–6], or a ferroelectric phase boundary, usually morphotropic phase boundary (MPB), can enhance the piezoelectricity [1–3,7]. The instability of the polarization at phase boundaries allows a significant polarization variation under an external stress or electric field, thus AC properties of materials can be enhanced [8,9]. A recent study [10] showed that properties can be further enhanced at a ferroelectric triple-point–type MPB (a triple point of a paraelectric cubic phase, a ferroelectric rhombohedral phase and a ferroelectric tetragonal phase coexisting) [10–13].

In this work, we reported a way to further enhance these AC properties in a lead-free ceramic: the piezoelectric coefficient d_{33} reaches 697 pC/N and relative dielectric permittivity has a giant value of ~ 75000. A new type phase-coexisting point, quasi-quadruple point, is proved to play an important role. Ferroelectric quasi-quadruple point (QP) characterizes a state of four phases (*e.g.*, cubic-tetragonal-orthorhombic-rhombohedra or C-T-O-R) nearly coexisting at one point in a temperature-composition phase diagram. These four phases merge at nearly one point tending to form a quadruple point (four-phase–coexisting point), but experimentally it is hard to tell whether these four phases coexist at exactly one point or not, thus we define it a quasi-quadruple–point phenomenon.

A QP can be found in a simple $BaTiO_3$ doped with $BaSnO_3$ ceramic. Its rough phase diagram has been reported before [14,15], but no one discussed the detail of phase coexisting and piezoelectric properties. Also, the relationship between ferroelectric phase configuration and its properties remains unclear. Our work systematically studied AC properties of $BaTiO_3$-$BaSnO_3$ ceramic (a QP system) and compared with a similar but non-QP system, a $BaTiO_3$-$CaTiO_3$ solid solution. The experimental results showed clearly that AC properties enhanced greatly at the quasi-quadruple point and its nearby regions. In order

(a) E-mail: yaodongy@mail.xjtu.edu.cn
(b) E-mail: ren.xiaobing@mail.xjtu.edu.cn

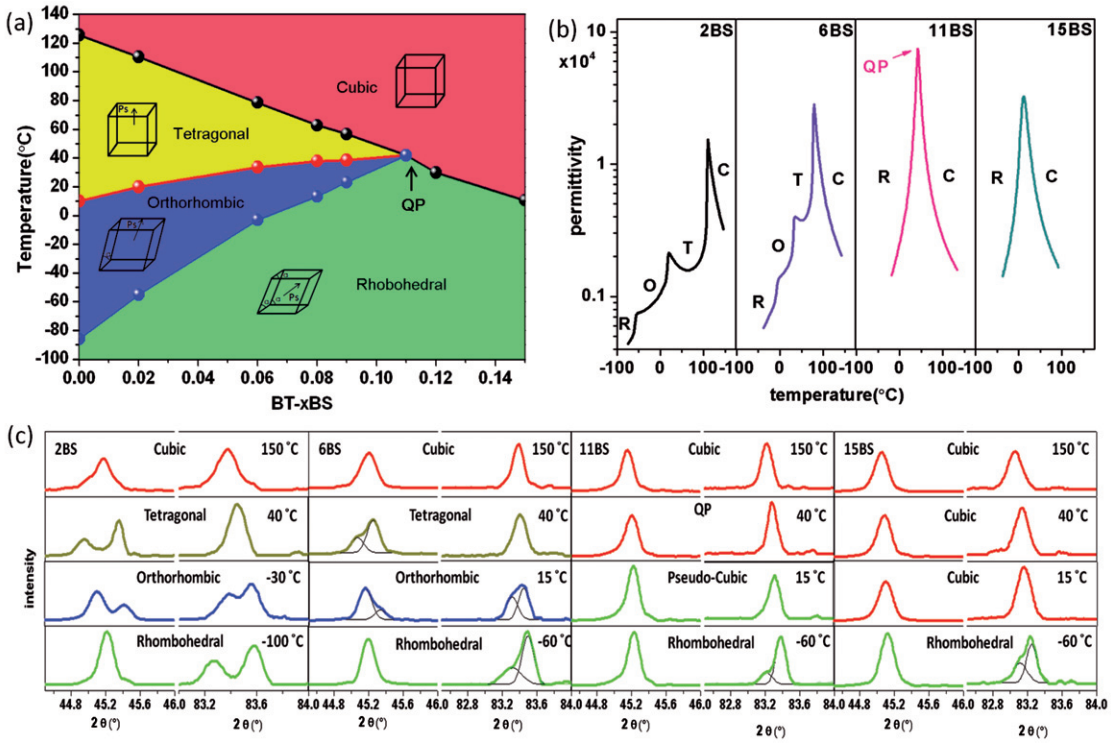

Fig. 1: (Color online) (a) Temperature-composition phase diagram of BT-xBS. Typical dielectric-temperature curves (b) and *in situ* XRD profiles (c) of BT-2BS, BT-6BS, BT-11BS and BT-15BS.

to understand this enhancement, the free-energy distributions are calculated via the Landau-Devonshire theory, which showed that the nearly vanishing of polarization rotation and extension energy barriers at QP is the reason of enhancement. The connection between phase configuration and its ferroelectric AC properties is built successfully in both experimental and theoretical aspects.

Samples were fabricated with the conventional solid-reaction method with starting materials of carbonate ($BaCO_3$) and oxide (TiO_2, SnO_2) powders with purities higher than 99.9% (Kanto Chemical Company). The calcination was performed at 1100 °C–1200 °C for 4 h and finally sintered at 1400 °C for 4 h in air. The structure was analyzed by a X-ray diffraction analysis meter (Shimadzu 7000 XRD). Dielectric constants were measured by a HIOKI LCR meter in the temperature range of −100 °C–150 °C (Delta chamber) at 1 kHz. The piezoelectric coefficient d_{33} was measured by a Burlincourt commercial d_{33} meter with a tunable temperature range from 0 °C to 80 °C.

Figure 1 shows the phase diagram of $BaTiO_3$-$x$$BaSnO_3$ (short as BT-xBS) determined by the dielectric permittivity measurement and XRD scan at different temperatures. In this phase diagram, the Curie temperature (T_c) decreases almost linearly with increasing Sn^{4+} dopants. T-O and O-R phase boundaries gradually merge with T_c lines and eventually these four C-T-O-R phases meet together at nearly one point around 42 °C with a composition of BT-11BS: a quasi-quadruple point formed. Figure 1(b) shows four typical dielectric permittivity curves of BT-xBS at different compositions ($x = 2$, 6, 11, 15). Phase transition routes of C-T-O-R (in both BT-2BS and BT-6BS), C through QP to R (in BT-11BS) and C directly to R (in BT-15BS) can be clearly found. Figure 1(c) is the *in situ* XRD line scan profiles of BT-2BS, BT-6BS, BT-11BS and BT-15BS during a cooling process. Both XRD and permittivity measurements coordinated with each other very well and demonstrated the same phase transition routes.

Figure 2 shows the AC properties of the BT-xBS system. Figure 2(a) is a contour map of the piezoelectric coefficient d_{33} in the BT-xBS temperature-composition plane, while the solid-point lines indicate the phase boundaries equal to those in fig. 1(a). Clearly, the gradient changes of d_{33} are in accordance with the phase configurations. d_{33} gets its maximum value of 697 pC/N at the quasi-quadruple point, which is a five-times enhancement compared with the value of pure BT and is also the largest reported value in Pb-free ceramics so far [7,10,16]. Shifting from QP, this value decreases with temperature and composition at different tendencies. For example, decreasing is precipitous in the upper-right zone of fig. 2(a) due to the fact that the material is entering the paraelectric phase. But decreasing is gradual in the bottom-left area, especially along T-O and O-R phase boundaries (two MPBs, see fig. 2(a) and (b)). At these two MPBs, BT-xBS has a better performance than at off-MPB regions and a QP always can generate at least two MPBs. From

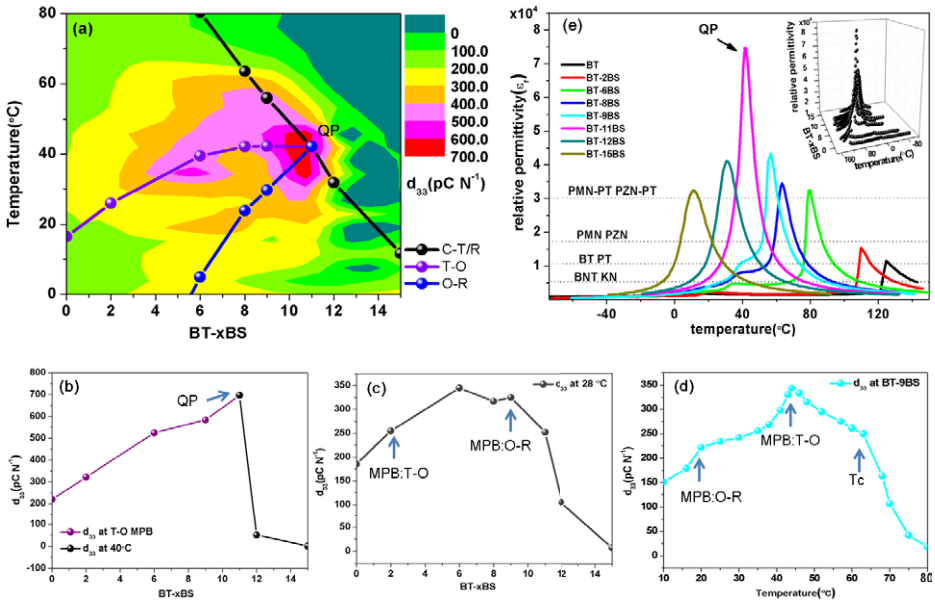

Fig. 2: (Color online) AC properties of BT-xBS ceramic: (a) contour map of the d_{33} coefficient in temperature-composition dimensions (the Renka-Cline method was used to form the gridding, the dotted lines indicate the phase diagram of BT-xBS); (b) d_{33}-composition curve along T-O MPB and at 40 °C (after entering the C phase); (c) d_{33}-composition curve at 28 °C; (d) d_{33}-temperature curve at BT-9BS; (e) dielectric permittivity-temperature curves of BT-xBS at different compositions (the dashed lines indicate permittivity values of some classical ferroelectric materials at T_c). The inset is the same diagram in a 3D view.

d_{33}-temperature (fig. 2(c)) and d_{33}-component (fig. 2(d)) line profiles, a very broad peak can be found. It is quite different from regular piezoelectric materials (*e.g.*, $Pb(Mg_{1/3}Nb_{2/3})O_3$-29$PbTiO_3$), which only have a very sharp and narrow peak in its d_{33}-temperature (or component) profile. A QP and two MPBs offer a broad region with high piezoelectric properties in the phase diagram, which allows piezoelectric materials to maintain high properties under a large-temperature (or composition, or both) region.

Please notice that d_{33} does not decrease to zero just above T_c, because when doped with more $BaSnO_3$, these samples have polarized nano-regions (PNRs) at a temperature above T_c, which have already been reported [14,17,18].

Figure 2(e) shows the permittivity curves of BT-xBS at different compositions and temperature. Similar as the d_{33} contour map (fig. 2(a)), dielectric permittivity reaches its maximum value 75000 at QP (fig. 2(e)). Compared with permittivity values of some classical ferroelectric ceramics at their T_c, *e.g.*, $BaTiO_3$(BT) [19], $PbTiO_3$(PT) [20], $(Bi_{0.5}Na_{0.5})TiO_3$(BNT) [21], $KNbO_3$(KN) [22], $PbMg_{0.33}Nb_{0.67}O_3$(PMN) [4], $PbZn_{0.33}Nb_{0.67}O_3$(PZN) [4], PMN-PT [23], PZN-PT [24] (values marked in fig. 2(e)), the permittivity of BT-xBS has a remarkable enhancement at QP. This value decreases quickly when composition or temperature leaving from the quasi-quadruple point, as can be clearly seen from the permittivity *vs.* temperature curves for different compositions in 3D (inset of fig. 2(e)).

The above result reveals the strong nonlinear change of AC properties with composition and temperature, which is highly related with its phase configurations: AC properties at QP are comparably larger than those at phase boundaries, and even larger than those at single phase. To further understand the mechanism and role of QP, two BT-based ceramics are chosen and compared in both properties and free-energy aspects. As mentioned above, a C-T-O-R phase coexisting quasi-quadruple point and two MPBs can be found in $BaTiO_3$ doped with Sn^{4+}. In contrast, there is only C-T, T-O, O-R phase boundaries, but no three or more phases coexisting point can be found in $BaTiO_3$ doped with Ca^{2+} (BT-xCT). Both BT-xBS and BT-xCT have two ferroelectric phase boundaries (T-O and O-R), but only BT-xBS forms a quasi-quadruple point. BT-xCT is prepared via a similar solid-state reaction as BT-xBS. (The phase diagram of BT-xCT can be found in ref. [25] and in the inserts of fig. 3.)

Permittivity values at T_c of these two ceramics are showed in fig. 3(a). It is obvious that QP plays a very important role to enhance the permittivity. In contrast, permittivity shows almost no change on the C-T boundary of BT-xCT. Permittivity values at T-O phase boundaries from these two materials are also shown in fig. 3(b). Again, the permittivity of a MPB (T-O boundary in BT-xBS) increases notably, but that of a polymorphic phase boundary (PPB, T-O boundary in BT-xCT) shows almost no change.

These are similar C-T and T-O phase boundaries in both BT-xBS and BT-xCT ceramics, but their

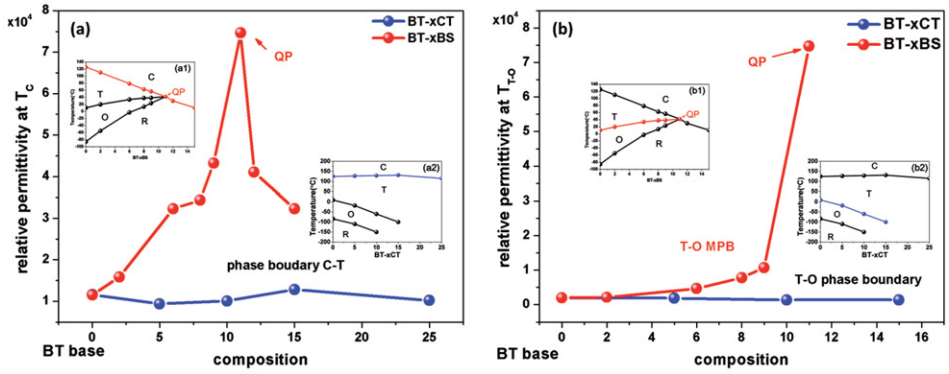

Fig. 3: (Color online) Permittivity comparison for different BT base ceramics: (a) permittivity-composition curves at T_c; (b) permittivity-composition curves at T-O phase boundaries. (The insets show the phase diagrams of BT-xBS and BT-xCT: (a1) and (b1) are phase diagrams of BT-xBS; (a2) and (b2) are phase diagrams of BT-xCT. Colored boundaries indicate where the permittivity data are taken from.)

permittivity values are very different. Why? To understand the origin of high performance related to QP, the free-energy descriptions for two above ceramics were calculated via Landau-Devonshire theory at different kinds of phase coexisting configurations. Up to 6th-order terms of polarization were considered and there is no strain coupling in this calculation. The equation of Landau-Devonshire theory in all three dimensions is given as follows [26–29]:

$$\begin{aligned} F(\vec{P}) \;=\; & F_0 + a(P_x^2+P_y^2+P_z^2) + b_1(P_x^4+P_y^4+P_z^4) \\ & + b_2(P_x^2P_y^2+P_y^2P_z^2+P_x^2P_z^2) + c_1(P_x^6+P_y^6+P_z^6) \\ & + c_2[P_x^4(P_y^2+P_z^2)+P_y^4(P_x^2+P_z^2)+P_z^4(P_x^2+P_y^2)] \\ & + c_3P_x^2P_y^2P_z^2. \end{aligned} \tag{1}$$

Parameters a, b_1, b_2, c_1, c_2, c_3, d are the coefficients for different orders of polarization P. F is the free energy at a certain temperature and composition as a function of polarization (F_0 means free energy of a paraelectric phase). At a phase coexisting point, the free energy of different phases should equal each other when they coexist and the first deviation of free energy for a certain phase should equal zero to make the phase stable (formula (2)). For the sake of simplicity, assume polarizations in three different ferroelectric phases have the same length but own different orientations:

$$\begin{aligned} &1)\quad F(\vec{P}_T)=F(\vec{P}_O)=F(\vec{P}_R)=F(\vec{P}_C)=F_0; \\ &2)\quad \frac{\partial F(\vec{P})}{\partial \vec{P}}=0 \quad (\text{at } \vec{P}=\vec{P}_T, \vec{P}=\vec{P}_R, \vec{P}=\vec{P}_O), \end{aligned} \tag{2}$$

where

$$\vec{P}_T = P_0*(0,0,1), \quad \vec{P}_O = P_0*\left(0, {}^1\!/\!_{\sqrt{2}}, {}^1\!/\!_{\sqrt{2}}\right),$$
$$\vec{P}_R = P_0*\left({}^1\!/\!_{\sqrt{3}}, {}^1\!/\!_{\sqrt{3}}, {}^1\!/\!_{\sqrt{3}}\right).$$

Based on these different phase coexisting conditions, the free-energy descriptions for different phase configurations can be rewritten as follows.

At a quadruple point (*e.g.*, C-T-O-R):

$$\begin{aligned} F(\vec{P}) \;=\; & F_0 + c_1P_0^4P^2 - 2c_1P_0^2P^4 + c_1P^6; \\ & (P^2 = P_x^2+P_y^2+P_z^2). \end{aligned} \tag{3}$$

At a PE-FE phase boundary (*e.g.*, C-T):

$$\begin{aligned} F(\vec{P}) \;=\; & F_0 + c_1P_0^4P^2 - 2c_1P_0^2P^4 + c_1P^6 \\ & + (b_2+4c_1P_0^2)(P_x^2P_y^2+P_y^2P_z^2+P_x^2P_z^2) \\ & + (c_2-3c_1)[P_x^4(P_y^2+P_z^2)+P_y^4(P_x^2+P_z^2) \\ & + P_z^4(P_x^2+P_y^2)] + (c_3-6c_1)P_x^2P_y^2P_z^2. \end{aligned} \tag{4}$$

At a FE-FE phase boundary (*e.g.*, T-O):

$$F(\vec{P}) = F_0 + aP^2 + b_1P^4 + c_1P^6 + (c_3-6c_1)P_x^2P_y^2P_z^2. \tag{5}$$

After plotting the free-energy profile, we can clearly see the difference (fig. 4). At quadruple point (eq. (3)), the free-energy distribution is a sphere (polarizations with same length), which means that the change of the polarization direction does not change the free energy and there is no energy barrier for polarization rotation between these different FE phases (fig. 4(a)). Due to the neutralization relationship between parameters of different orders, the total free energy is relatively stable for the length change of polarizations at one direction, the energy barrier for polarization extension between PE and FE phases is rather small (fig. 4(e)). This low energy barrier can greatly facilitate the polarization rotation and extension as proposed by Damjanovic [30]. At C-T phase boundaries, free energies possess the 4th- and 6th-order anisotropy (eq. (4)), thus there are energy barriers between FE-FE rotation (fig. 4(b)) and PE-FE extension (fig. 4(f)), AC properties at C-T or C-R are not as good as at QP. This is the main reason to enhance AC properties at QP in BT-xBS ceramic (see figs. 2(a), 2(e), 3(a) for experimental results).

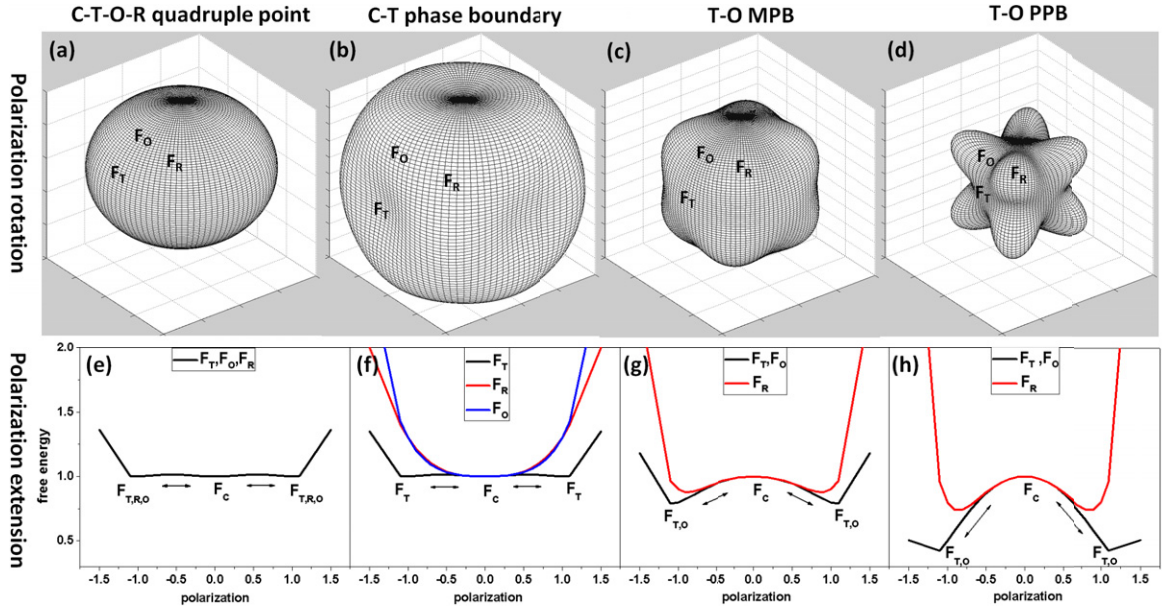

Fig. 4: (Color online) Schematic diagram of the free-energy profile for a ferroelectric system under different situations: upper panels ((a)–(d)) are the free-energy profiles for different polarizations with $|P| = P_0$ (polarization rotation case); bottom panels ((e)–(h)) are the free-energy profiles for different polarizations in T, R, O direction (polarization extension case). Each column relates to a different phase configuration: ((a), (e)) C-T-O-R quadruple point; ((b), (f)) C-T phase boundary; ((c), (g)) T-O MPB; and ((d), (h)) T-O PPB. (Plot values and parameters can be found in footnote [1]).

At a T-O boundary, the free-energy expression not only has 6th-order anisotropy, but also has large energy barriers for polarization extension. There are two different cases: when going via a T-O boundary toward the quadruple point, its free-energy landscape will change to fig. 4(a). Since there is a R phase coexisting in the neighbor region, the energy gap between the R phase and the T (or O) phase is small (fig. 4(c)). In another case, without a quadruple point, the energy gap is high (fig. 4(d)). This is exactly what happened in the permittivity measurement (fig. 3(b)). At the beginning, permittivities on these two T-O phase boundaries of BT-xBS and BT-xCT are almost the same. But as dopants increase, T-O MPB of BT-xBS goes up to reach a quasi-quadruple point, which indicates that the energy difference between the T (O) phase and other two phases (C and R) gradually vanishes, while T-O PPB of BT-xCT goes down to a lower temperature, which increases the energy difference between the T (O) and C phases.

Based on the Landau-Devonshire theory analysis, our theoretical calculation matched the experimental result, which gave a strong proof that the origin of the AC properties enhancement at QP comes from decreasing energy barriers for polarization rotation and extension induced by phase coexisting. It is also worth noticing that this is the first experimental work to reveal lowering energy barriers for both polarization rotation and extension to enhance the piezoelectricity after what predicted by Damjanovic [30]. It is clear that polarization extension plays an important role to affect these AC properties.

A ferroelectric quasi-quadruple point could obviously enhance AC properties, such as permittivity and piezoelectricity. A quasi-quadruple point and double MPBs together opened a large window to maintain a high piezoelectricity in wide composition and temperature ranges. These distinctive AC properties enhancements at QP are the result of nearly vanishing energy barriers for both polarization rotation and extension.

* * *

Authors are grateful to other MMRC members for useful discussions. This work is supported by the Ministry of Science and Technology of China through a 973-Project under Grant No. 2012CB619401 and National Natural Science Foundation of China (Grant Nos. 50720145101, 51072158 and 50771079).

[1] Parameters for the schematic diagram (these parameters were chosen according to the relation between them as well as the phase-coexisting situation consideration): quadruple point C-T-O-R ($f_0 = 1$; $p_0 = 1$; $c_1 = 0.1$; $b_1 = -2 * c_1 * p_0^2$; $a = c_1 * p_0^4$; $b_2 = 2 * b_1$; $c_2 = 3 * c_1$; $c_3 = 6 * c_1$); phase boundary C-T ($f_0 = 1; p_0 = 1; c_1 = 0.1$; $b_1 = -2 * c_1 * p_0^2$; $a = c_1 * p_0^4$; $b_2 = 1$; $c_2 = 0.1$; $c_3 = -2.4$); MPB T-O ($f_0 = 1$; $p_0 = 1$; $c_1 = 0.1$; $b_1 = -0.1$; $a = -0.2$; $b_2 = 2 * b_1$; $c_2 = 3 * c_1$; $c_3 = 3.8$); phase boundary T-O ($f_0 = 1$; $p_0 = 1; c_1 = 0.1$; $b_1 = -0.1; a = -0.5$; $b_2 = 2 * b_1$; $c_2 = 3 * c_1$; $c_3 = 10.2$).

REFERENCES

[1] Jaffe B., Cook W. R. and Jaffe H., *Piezoelectric Ceramics*, Vol. **1** (Academic Press, London) 1971.
[2] Uchino K., *Ferroelectric Devices*, Vol. **16** (CRC) 2000.

[3] Lines M. E. and Glass A. M., *Principles and Applications of Ferroelectrics and Related Materials* (Oxford University Press, USA) 2001.
[4] Cross L. E., *Ferroelectrics*, **76** (1987) 241.
[5] Cross L. E., *Ferroelectrics*, **151** (1994) 305.
[6] Merz W. J., *Phys. Rev.*, **76** (1949) 1221.
[7] Rödel J. *et al.*, *J. Am. Ceram. Soc.*, **92** (2009) 1153.
[8] Fu H. and Cohen R., *Nature*, **403** (2000) 281.
[9] Ahart M. *et al.*, *Nature*, **451** (2008) 545.
[10] Liu W. and Ren X., *Phys. Rev. Lett.*, **103** (2009) 257602.
[11] Bao H. *et al.*, *J. Phys. D: Appl. Phys.*, **43** (2010) 465401.
[12] Xue D. *et al.*, *Appl. Phys. Lett.*, **99** (2011) 122901.
[13] Xue D. *et al.*, *J. Appl. Phys.*, **109** (2011) 054110.
[14] Lei C., Bokov A. A. and Ye Z.-G., *J. Appl. Phys.*, **101** (2007) 084105.
[15] Yasuda N., Ohwa H. and Asano S., *Jpn. J. Appl. Phys.*, **35** (1996) 5099.
[16] Saito Y. *et al.*, *Nature*, **432** (2004) 84.
[17] Lu S. G., Xu Z. K. and Chen H., *Appl. Phys. Lett.*, **85** (2004) 5319.
[18] Bokov A. A. and Ye Z. G., *J. Mater. Sci.*, **41** (2006) 31.
[19] Kinoshita K. and Yamaji A., *J. Appl. Phys.*, **47** (1976) 371.
[20] Remeika J. and Glass A., *Mater. Res. Bull.*, **5** (1970) 37.
[21] Smolenskii G. *et al.*, *Sov. Phys. Solid State*, **2** (1961) 2651.
[22] Shirane G., Newnham R. and Pepinsky R., *Phys. Rev.*, **96** (1954) 581.
[23] Choi S. *et al.*, *Ferroelectrics*, **100** (1989) 29.
[24] Nomura S., Arima H. and Kojima F., *Jpn. J. Appl. Phys.*, **12** (1973) 531.
[25] Mitsui T. and Westphal W. B., *Phys. Rev.*, **124** (1961) 1354.
[26] Landau L., *Nature*, **138** (1936) 840.
[27] Falk F., *J. Phys. Colloques*, **43** (1982) C4-3.
[28] Sergienko I., Gufan Y. M. and Urazhdin S., *Phys. Rev. B*, **65** (2002) 144104.
[29] Khachaturyan A. G., *Philos. Mag.*, **90** (2010) 37.
[30] Damjanovic D., *Appl. Phys. Lett.*, **97** (2010) 062906.